

## 2D-Empowered 3D Object Detection on the Edge

JINGZONG LI, City University of Hong Kong, China  
 YIK HONG CAI, The Chinese University of Hong Kong, China  
 LIBIN LIU, Zhongguancun Laboratory, China  
 YU MAO, City University of Hong Kong, China  
 CHUN JASON XUE, City University of Hong Kong, China  
 HONG XU, The Chinese University of Hong Kong, China

3D object detection has a pivotal role in a wide range of applications, most notably autonomous driving and robotics. These applications are commonly deployed on edge devices to promptly interact with the environment, and often require near real-time response. With limited computation power, it is challenging to execute 3D detection on the edge using highly complex neural networks. Common approaches such as offloading to the cloud brings latency overheads due to the large amount of 3D point cloud data during transmission. To resolve the tension between wimpy edge devices and compute-intensive inference workloads, we explore the possibility of transforming fast 2D detection results to extrapolate 3D bounding boxes. To this end, we present Moby, a novel system that demonstrates the feasibility and potential of our approach. Our main contributions are two-fold: First, we design a 2D-to-3D transformation pipeline that takes as input the point cloud data from LiDAR and 2D bounding boxes from camera that are captured at exactly the same time, and generate 3D bounding boxes efficiently and accurately based on detection results of the previous frames without running 3D detectors. Second, we design a frame offloading scheduler that dynamically launches a 3D detection when the error of 2D-to-3D transformation accumulates to a certain level, so the subsequent transformations can draw upon the latest 3D detection results with better accuracy. Extensive evaluation on NVIDIA Jetson TX2 with the autonomous driving dataset KITTI and real-world 4G/LTE traces shows that, Moby reduces the end-to-end latency by up to 91.9% with mild accuracy drop compared to baselines. Further, Moby shows excellent energy efficiency by saving power consumption and memory footprint up to 75.7% and 48.1%, respectively.

**CCS Concepts:** • Human-centered computing → Ubiquitous and mobile computing systems and tools; • Computer systems organization → Robotics.

Additional Key Words and Phrases: 3D object detection, robotics application, edge computing, on-device acceleration

### ACM Reference Format:

Jingzong Li, Yik Hong Cai, Libin Liu, Yu Mao, Chun Jason Xue, and Hong Xu. 2023. 2D-Empowered 3D Object Detection on the Edge. 1, 1 (February 2023), 23 pages. <https://doi.org/10.1145/nnnnnnnn.nnnnnnn>

### 1 INTRODUCTION

The rapid development of Deep Neural Networks (DNNs) has empowered a number of usecases, including object detection, face recognition and image super-resolution [27, 28, 73]. One of the most promising usecases is 3D object detection, which plays a pivotal role in a wide range of applications such as robotics and autonomous driving that require accurate perception of their surrounding environment to operate well [15, 55]. 3D object detection is a fundamental basis in these perception systems, and significant research effort has been devoted to improving its accuracy [42, 58, 59, 62, 71, 72]. It takes 3D sensory data represented by point clouds as input that is generally captured by LiDAR, to generate 3D bounding boxes. An example is illustrated in Fig. 1. Compared to

---

Authors' addresses: Jingzong Li, [jingzong.li@my.cityu.edu.hk](mailto:jingzong.li@my.cityu.edu.hk), City University of Hong Kong, Hong Kong, China; Yik Hong Cai, [1155141377@link.cuhk.edu.hk](mailto:1155141377@link.cuhk.edu.hk), The Chinese University of Hong Kong, Hong Kong, China; Libin Liu, [liu.libin@outlook.com](mailto:liu.libin@outlook.com), Zhongguancun Laboratory, Beijing, China; Yu Mao, [ymao7-c@my.cityu.edu.hk](mailto:ymao7-c@my.cityu.edu.hk), City University of Hong Kong, Hong Kong, China; Chun Jason Xue, [jasonxue@cityu.edu.hk](mailto:jasonxue@cityu.edu.hk), City University of Hong Kong, Hong Kong, China; Hong Xu, [hongxu@cuhk.edu.hk](mailto:hongxu@cuhk.edu.hk), The Chinese University of Hong Kong, Hong Kong, China.

---

its 2D counterpart, 3D object detection introduces a third dimension to characterize the location and size of an object in the real world. Besides, 3D detection provides a heading angle that indicates orientation. Due to the task complexity and large amount of data to process, 3D detection models usually have more complicated structures with inflated model sizes, hence posing a higher demand for computation resources. We experimentally find that with the same hardware platform, the inference latency of 3D detection model can be up to 41 $\times$  of the 2D model (§2.2).

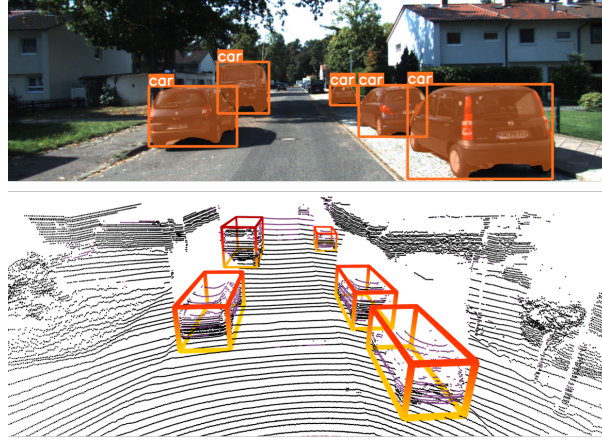


Fig. 1. 2D object detection VS 3D object detection

Meanwhile, with the proliferation of edge computing, robotics and autonomous driving applications are latency-sensitive and commonly deployed on edge devices to interact with its surrounding environment promptly [25, 39, 60, 64]. Although it is close to the data sources, edge computing is provisioned with limited computation power. Take the most commonly used edge device NVIDIA Jetson TX2 [11] as an example, the desktop-class GPU RTX 2080Ti has 17 $\times$  more CUDA cores than TX2 [5], and the number even soars to 31 $\times$  for the high-end GPU Tesla A100 [6]. Thus, it is notoriously difficult to run heavy 3D detection models on the resource-constrained edge devices for near real-time processing.

To ease this tension between constrained supply and growing demand for computing resources, the de-facto standard, cloud-only approach offloads the compute-intensive 3D object detection to the cloud for inference. Computation offloading shifts the heavy burden to the cloud and offers significant improvement of inference latency with the help of powerful servers. However, we find that the end-to-end latency is still not satisfactory for practical use, due to the transmission delay that accounts for the majority of the latency and bottlenecks the entire pipeline. As will be shown in §2.2, it requires nearly 300ms to transmit a point cloud file with an average size of 6.96Mb even under a high-speed cellular network. Yet point cloud can be compressed by using existing compression techniques, the non-negligible compression overhead still hinders providing near real-time 3D detection for robotics and autonomous driving applications.

Motivated by these limitations of edge- and cloud-only inference, and the drastically low inference time of 2D object detection, we present Moby, a new framework for accelerating 3D object detection on edge devices. Moby explores the possibility of using 2D models to extrapolate the 3D bounding boxes. The key insight behind Moby is that, instead of launching heavy DNN-based 3D detectors completely on edge or cloud, we can devise a light-weight *transformation* method that can effortlessly run on board, and only a few anchor frames that require accurate 3D object detection are offloaded to server for inference. Precisely, we propose a light-weight 2D-to-3D transformation approach that can construct 3D bounding boxes based on outputs from 2D model. This

transformation enables Moby to generate 3D detection results on board in near real-time, without running 3D models that are ill-suited for edge computing.

Creating such a full-fledged system that achieves 3D object detection in a near real-time manner, however, needs to deal with two key challenges: (1) At the frame level, how can Moby accurately and efficiently transform 2D bounding boxes into 3D ones, thus maximizing the latency benefit from 2D detection? (2) Across frames, as the error of 2D-to-3D transformation accumulates over time, how can Moby monitor the accuracy drop and decide the offloading timing for accurate DNN-based 3D detection? Moby addresses these two challenges by introducing a novel system design. First, Moby starts by running a fast on-board instance segmentation model to obtain both 2D detections and segmentation masks. To utilize previous 3D detection results for better transformation, a *tracking-based association* component is designed to establish the association of 2D bounding boxes in adjacent frames. Next, we propose the *2D-to-3D Transformation* component, which is a light-weight geometric method that takes in both 2D results and point cloud to generate 3D bounding boxes efficiently. Specifically, we transfer semantic information contained in the segmentation masks to point cloud to obtain the point cluster of each potential object. Point filtration is designed to eliminate tainted points in each cluster. Then we design a sequence of geometric methods to accurately construct 3D bounding boxes by referring to previous detection results. Finally, as the error of transformation accumulates over time, a *frame offloading scheduler* is designed to judiciously decide when to offload a new frame to launch DNN-based 3D detection timely for the subsequent transformation to utilize.

We evaluate Moby using a full system implementation on an NVIDIA Jetson TX2 and a desktop server equipped with RTX 2080Ti GPU. We evaluate Moby with the most well-known autonomous driving dataset, KITTI [32], which provides real LiDAR scans and camera frames to evaluate 3D object detection. Compared to existing 3D approaches, Moby offers up to 91.9% end-to-end latency reduction while compromising only modest accuracy loss. Remarkably, Moby can even achieve 10 fps on Jetson TX2 that matches the scanning frequency of KITTI’s LiDAR. Our evaluation results also reveal that Moby is able to curtail power consumption and memory usage by up to 75.7% and 48.1%, respectively. That is extremely vital for constrained edges to save resources for more urgent computation tasks.

In summary, we make three key contributions:

- We comprehensively investigate the system challenges of deploying existing 3D detection models on edge or cloud. We experimentally reveal that edge- and cloud-only inference severely suffers from unacceptable on-board latency and transmission bottlenecks, respectively.
- We build Moby, the first system that enables such 2D-to-3D transformation for robotics and autonomous driving applications. Moby creatively incorporates previous detection results to assist the transformation. Besides, we propose a novel way to orchestrate the edge and cloud computation for 3D object detection with a frame offloading scheduler.
- Our experiments demonstrate that Moby offers a significant latency reduction by up to 91.9% against several state-of-the-art 3D object detection models, while only compromising modest accuracy loss.

## 2 BACKGROUND AND MOTIVATION

### 2.1 The Need for 3D Object Detection

Object detection has gained tremendous attention from researchers in the computer vision community, especially the 2D object detection methods, which normally apply DNNs to extract 2D bounding boxes on the image plane. Although state-of-the-art 2D detection techniques can detect objects with high accuracy, they lack the depth information to localize objects and estimate their size, which is essential for tasks like path planning and collision avoidance in robotics and autonomous driving [15, 55]. To overcome these limitations, 3D object detection

methods are proposed. Fig. 1 depicts the difference between 2D and 3D object detection. 3D detection provides a third dimension to characterize the object size and position in world coordinates.

Generally, 3D object detection falls into one of three approaches based on the input modality [15]. The first approach uses the point cloud data from LiDAR sensors to generate 3D bounding boxes [42, 58, 59, 62, 72, 80]. The second one is image-based [20, 50, 56, 70, 74] that use neural networks to recover the depth information from image planes for 3D bounding boxes. The images are generally captured by monocular cameras that are cheap and much more accessible in many situations. Naturally, this approach has accuracy gaps due to errors in depth recovery from 2D to 3D compared to the point cloud approach [55]. The third approach is fusion-based [21, 22, 53, 54, 68, 71] which takes both image and point cloud data as inputs to improve performance.

Despite the rapid development of image- and fusion-based methods, they still lag behind the point cloud approach to date [55]. As of January 2023, nine of the top ten methods on the popular KITTI leaderboard [2] are point cloud-based. Unless otherwise noted, we adopt point cloud-based methods for 3D object detection.

## 2.2 Challenges of 3D Detection on the Edge

Despite advancements in hardware and deep neural networks [15, 55], performing 3D detection is still a daunting task for resource-constrained edge devices such as vehicles and robots compared to the cloud [18]. Meanwhile, detection needs to be done frequently enough to keep track of the moving objects, which requires short detection/inference time on the device.

To clearly illustrate the challenges, we measure the inference latency of 3D object detection models on a typical edge device, NVIDIA Jetson TX2 [11], with one 256-core Pascal GPU. To experiment with offloading the 3D object detection models to the cloud, we build a testbed to run the models using a GPU server and replay the real-world network traces to emulate the wide-area network conditions. To profile the inference latency on edge devices, we select four commonly-used point cloud-based models, as summarized in Table 1.

**Edge-only inference.** We run these models on a Jetson TX2 using the KITTI dataset [32], the most popular dataset in the field of autonomous driving, and apply OpenPCDet [65] as the inference engine. The edge-only on-device inference results are shown in Fig. 2(a).

Model	PointPillar	SECOND	PointRCNN	PV-RCNN
Feature Extraction	Voxel based	Voxel based	Point based	Point-voxel based
Network Architecture	One Stage	One Stage	Two Stages	Two Stages

Table 1. Point cloud-based models we use. PointPillar [42] and SECOND[72] group points into vertical columns or voxels and apply convolution over these structures; PointRCNN[59] extracts features directly from the points with permutation invariant learning; PV-RCNN[58] combines the point and voxel features.

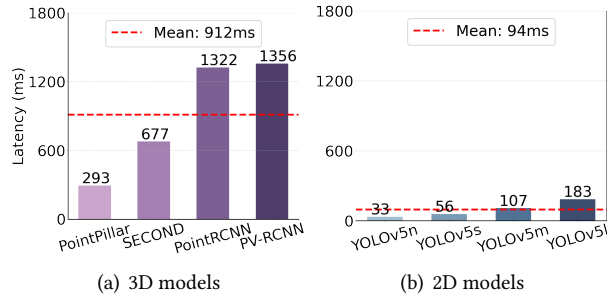


Fig. 2. The end-to-end latency of edge-only inference.

We observe that: (i) The average on-device inference latency reaches 912ms across the models, which is impractical for real-world applications that need to respond to the environment promptly; (ii) Even the one-stage models (PointPillar and SECOND) that classify bounding boxes in one step without pre-generated region proposals, take 293ms and 677ms on average, respectively; unsurprisingly, two-stage approaches take longer due to their more complicated pipelines.

To better understand the high computational cost of 3D models, we also compare them against 2D detection models. We use four YOLOv5 [33] variants.<sup>1</sup> The input images also come from the KITTI dataset [32] and are captured by its car camera with a resolution of 1242×375. Observe from Fig. 2(b) that the on-device inference latency of 2D models is much shorter. Notably, YOLOv5n only takes 33ms on average; even for the largest YOLOv5l, the inference latency is only 62% of the fastest 3D model PointPillar.

**Cloud-only inference.** Due to the high latency of edge-only inference, naturally one considers the possibility of performing the inference tasks in the cloud with much more powerful hardware. However, with an average size of 6.96Mb per file, streaming point cloud data to the cloud is bandwidth-intensive and offsets the inference latency savings. To estimate the end-to-end latency of cloud-only inference, we simulate the network conditions with empirical 4G/LTE bandwidth traces of the FCC [30] and Belgium [67] datasets. The four traces are summarized in Table 3. The point cloud data is uploaded to the server using one TCP connection, and Linux TC [7] is used to throttle the link capacity according to the bandwidth traces. The server performs 3D detection on an RTX 2080Ti GPU. Note that we deliberately select the traces that cover different parts of the bandwidth spectrum, and they are all within a normal 4G/LTE cellular performance ( $\sim 10\text{--}30\text{Mbps}$ ) [1]. It is likely that the real-world performance of cloud-only inference could be worse than what we report here in certain environments [73].

Trace (Mbps)	Mean ( $\pm$ Std)	Range	$P_{25\%}$	Median	$P_{75\%}$
FCC-1	11.89 ( $\pm 2.83$ )	[7.76, 17.76]	9.09	12.08	13.42
FCC-2	16.69 ( $\pm 4.69$ )	[8.824, 28.157]	13.91	16.07	19.43
Belgium-1	23.89 ( $\pm 4.93$ )	[16.02, 33.33]	19.84	23.46	27.73
Belgium-2	29.60 ( $\pm 4.92$ )	[20.17, 37.345]	25.18	30.761	32.76

Fig. 3. Statistics of four cellular bandwidth traces.

Algorithm	gzip	zlib	bzip2	lzma
Compression Time (ms)	134	238	1007	1179
Compression Ratio	1.57	1.57	1.75	1.83

Table 2. The latency and compression ratio of four common compression algorithms.

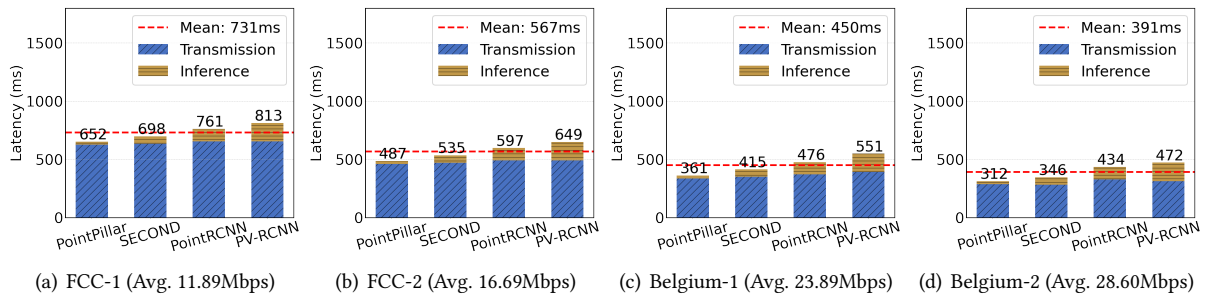


Fig. 4. The end-to-end latency of cloud-only inference on four real-word network traces.

As shown in Fig. 4, we observe that: (1) Even for trace with the highest average bandwidth, Belgium 2, the average end-to-end latency reaches 391ms across four models. This is much better than edge-only latency with 912ms mean latency, but it is still not satisfactory for practical use. (2) The transmission delay over the wide Internet accounts for the majority of inference time. When the network condition deteriorates, the end-to-end latency grows noticeably: For example, the inference time with FCC-1 trace is almost twice that of Belgium-2. In

<sup>1</sup>Here we use instance segmentation models in YOLOv5’s official release, which can output detection results and segmentation masks all at once and are consistent with our following design.

addition, we also consider compressing the point cloud data before transmission. We test the performance of four representative compression algorithms: gzip [4], zlib [14], bz2 [3] and lzma [8] on TX2, whose CPU runs at 2GHz. We use the implementation in Python standard library to run these algorithms on 50 point cloud files and report the average. The results are presented in Table. 2. We observe that the compression time is all above 100ms, and a larger compression ratio results in a longer time. With the fastest algorithm gzip, it can reduce the end-to-end latency of the slowest FCC-1 by 78ms. While for higher bandwidth traces, the compression does not contribute to the latency reduction much and can even jeopardize it. Based on these results, it is evident that offloading all 3D frames to cloud for inference is also impractical.

### 2.3 Using 2D Models for 3D Detection

We observe from the above experiments that the bottleneck of 3D object detection lies in the sheer amount of data that either needs to be processed by complex models on the wimpy edge, or to be transmitted over cellular networks to the cloud. Motivated by the drastically lower inference time of 2D object detection (recall Fig. 4) and the close correspondence between the 2D and 3D bounding boxes (recall Fig. 1), we cannot help but wonder: what if we use 2D detection models to extrapolate the 3D bounding boxes? Evidently, we need to start the process with DNN-based 3D detection on a certain LiDAR frame, i.e., an anchor frame, so we have information about the third dimension. Right after this, however, given the temporal similarity of adjacent LiDAR frames and the close correspondence between 3D and 2D projections, 2D detection can be sufficient to effectively infer the 3D results within a reasonable time window. Furthermore, previous detection results of anchor frame can be incorporated to perform better transformation. To our best knowledge, these have not been explored before.

The central tradeoff we need to balance here is between accuracy and latency. The more 2D detection we use, the more latency gain we can reap, but the accuracy will be lower as the 2D-to-3D mapping becomes more unreliable with time. Thus, we build Moby to attack two fundamental design questions on 2D-empowered 3D detection: (1) At the frame level, how can Moby transform a 2D bounding box to a 3D one accurately and efficiently, so we can maximize the latency benefit from 2D detection? (2) Across frames, as the error from 2D-to-3D transformation accumulates over time, inevitably Moby has to launch 3D detection on a new anchor frame for the subsequent transformations to utilize. But how can Moby detect the accuracy drop timely and efficiently, since this entails comparing to the 3D detection results?

## 3 SYSTEM DESIGN

We now present the detailed design of Moby as a novel pipeline that effectively realizes 2D-empowered 3D detection. Following the system overview, we elaborate on Moby’s main components according to the workflow of its pipeline for ease of understanding. We emphasize the new problems introduced by Moby and our solutions in explaining each component, while keeping the description succinct for the well-understood tasks that are necessary for the pipeline.

### 3.1 System Overview

Fig. 5 illustrates the overall design of Moby. We summarize its workflow into three stages as highlighted in the figure: (1) **Preparation**. At time  $t$ , the edge device offloads the LiDAR frame  $P_t$  (i.e. point cloud), i.e. an anchor frame, to the cloud for 3D object detection, and obtains the 3D bounding boxes to initiate the process. The 3D bounding boxes are then projected to 2D ones on the image plane (steps 1 and 2 in Fig. 5). (2) **Transformation**. In the next time slot  $t + 1$ , the edge has both a new LiDAR frame  $P_{t+1}$  and image  $M_{t+1}$  from the camera. Instead of running 3D detection on  $P_{t+1}$  again, Moby runs an instance segmentation model on  $M_{t+1}$  and obtains the 2D bounding boxes and segmentation masks. The 2D bounding boxes of both  $M_{t+1}$  and  $M_t$  are fed into the *tracking-based association* module to build a mapping between the same objects in these two image frames, which

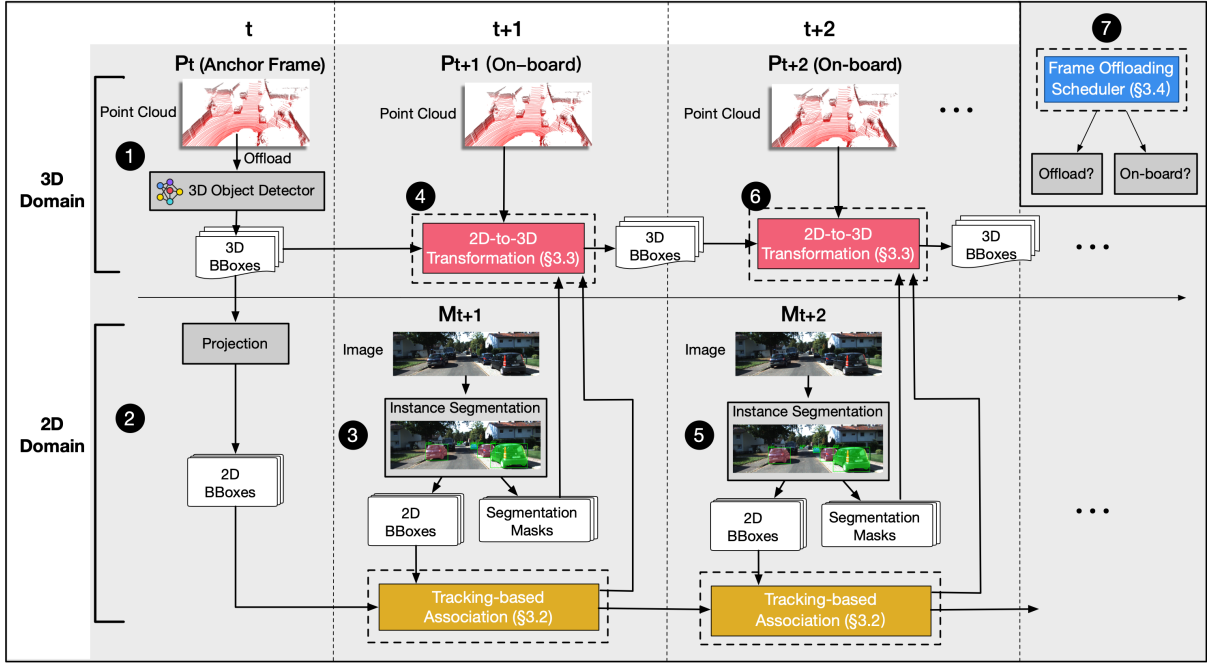


Fig. 5. Moby system overview.

serves as the basis for extrapolating the new positions of the corresponding 3D bounding boxes on  $P_{t+1}$  based on  $P_t$ . Then, using 3D bounding boxes from  $P_t$  as the reference, the *2D-to-3D transformation* module applies this detection mapping and the segmentation masks to generate 3D bounding boxes on  $P_{t+1}$  (steps 3 and 4). The processing at  $t+2$  is identical by using detection mapping and 3D bounding boxes from  $t+1$  as the reference (steps 5 and 6). (3) **Scheduling**. Moby's 2D-empowered 3D detection inevitably causes accuracy drop especially as time goes. Thus it relies on a *scheduler* to efficiently monitor the quality of 2D-to-3D transformation and judiciously decide when to offload a new anchor frame to the cloud so the subsequent transformations have the most recent 3D information to draw upon.

We now introduce these components in detail.

### 3.2 Tracking-based Association

The goal of tracking-based association is to utilize tracking in the 2D domain to build the mappings between bounding boxes of the same object in two adjacent frames, which serves as a key basis for 2D-to-3D transformation. Fig. 6 shows an overview of tracking-based association.

**On-device 2D Inference.** First Moby needs to obtain the 2D bounding boxes on the current image. In case the current LiDAR frame is selected as an anchor frame for 3D detection, Moby directly projects the 3D results to 2D. Otherwise, Moby needs to run a 2D detection model. Here we choose instance segmentation models as they output both bounding boxes and segmentation masks at the same time. The bounding boxes are used in tracking below, while segmentation masks are needed for the 2D-to-3D transformation in §3.3.

**Kalman Filter-based Tracking.** Considering the limited computation resources of edge devices, the tracking module must: 1) introduces little latency overhead that can run on edge devices in real time, 2) while accurately tracking the inter-frame 2D bounding boxes to form a solid association between adjacent frames. We extensively

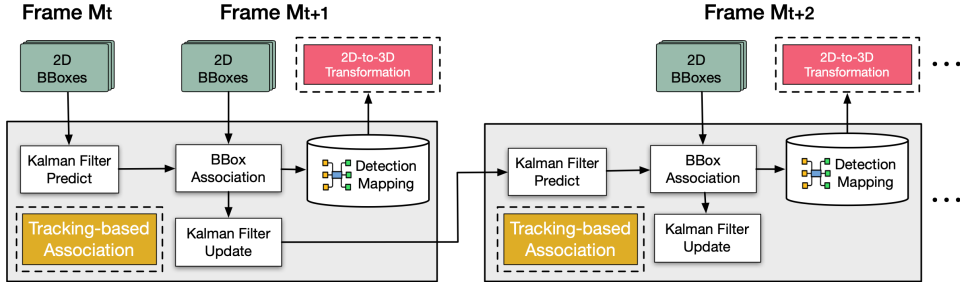


Fig. 6. Overview of tracking-based association.

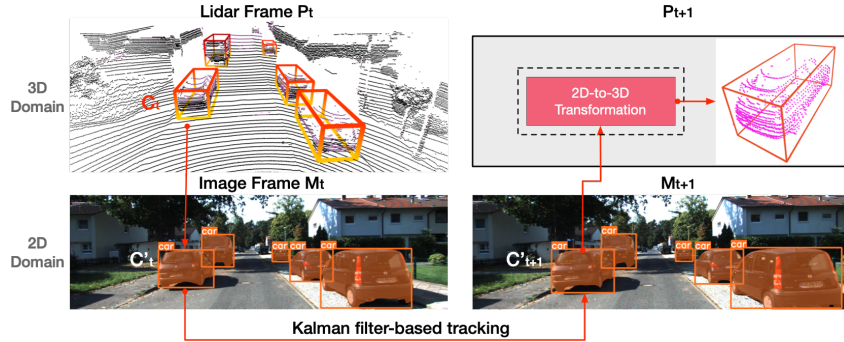


Fig. 7. Illustration of tracking and detection mapping.

explore existing object tracking techniques in pixel domain and adopt Kalman filter-based tracking [17], which satisfies both requirements. Kalman Filter is not only fast with simple algorithm [17] but also able to smooth the sizes and locations of boxes for better association, which makes the tracking more robust. The tracking pipeline is shown in Fig. 6: First, bounding boxes are detected in each frame. Then we apply a Kalman filter to predict the trajectories from the frame  $M_t$  to  $M_{t+1}$  and estimate the position of bounding boxes of each object in frame  $M_{t+1}$ . Next, we match the predicted boxes from Kalman filter with the 2D detection results on  $M_{t+1}$  by using the classic Hungarian algorithm [41]. The Intersection-over-Union (IoU) between two boxes is adopted as the matching criterion: If the detection to target overlap is less than an IoU threshold, association will be rejected. The Kalman filter then updates the trajectory prediction using the matched detections.

An example of tracking is illustrated in Fig. 7. The 2D boxes  $C'_t$  and  $C'_{t+1}$  from two adjacent frames are successfully associated, and Moby can further associate  $C'_{t+1}$  with the 3D bounding box  $C_t$  from the previous LiDAR frame. This detection mapping is stored to assist the following 2D-to-3D transformation.

### 3.3 2D-to-3D Transformation

We now discuss the 2D-to-3D transformation of bounding boxes, which is one of our main technical contributions along with the offloading scheduler design in §3.4. Fig. 8 shows an overview of the 2D-to-3D transformation. To incorporate 2D semantic information into 3D, Moby first projects the point cloud to the 2D segmentation masks of the image frame in the same time slot. The point cluster of each object can be identified in 3D. Moby further filters out points of the background that are erroneously labeled as objects. Finally, Moby relies on a light-weight geometric method, which leverages previous detection results as reference, to estimate 3D bounding boxes based on point clusters without running heavy 3D models.

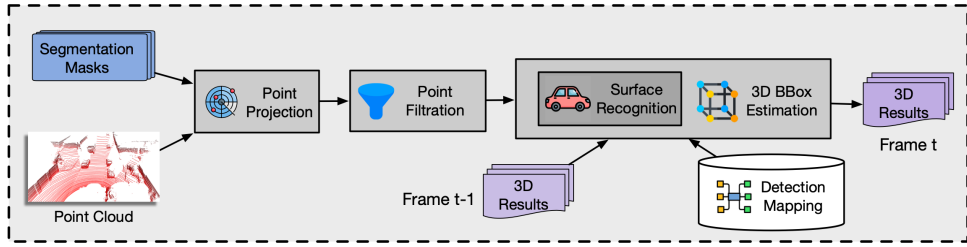


Fig. 8. Overview of 2D-to-3D transformation.

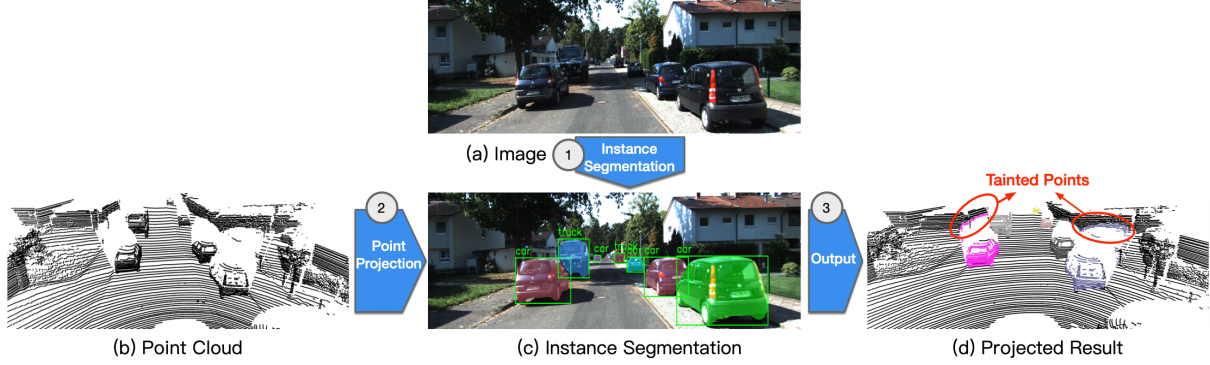


Fig. 9. An example of point projection on the KITTI dataset.

**Point Projection.** As discussed in §2.3, the 3D and 2D frames captured at the same time have closely related semantic information. To transfer the semantic information contained in the segmentation masks to 3D, we naturally choose to project the LiDAR frame to 2D domain. This projection is time-invariant since the camera and LiDAR are both fixed once they are installed, and the multimodal-sensor systems today usually provide the transformation matrices in the sensor calibration file. We again take the KITTI dataset [32] as an example. The transformation is as follows:

$$B = T_t * T_r * A. \quad (1)$$

Here  $A$  is points in 3D coordinate. They are first projected to a reference camera by the matrix  $T_r$ , and then projected to the target camera by  $T_t$ . With the corresponding 2D projection, we can then mark each 3D point to indicate which object it belongs to based on the segmentation masks, by squeezing the stacked masks along the channel dimension. Then the point cluster of each potential object can be identified. Fig. 9 illustrates the process and Fig. 9(d) shows the result with point clusters highlighted as parts of vehicles.

**Point Filtration.** Directly transferring segmentation masks to the point cloud may cause certain points to be erroneously marked as objects of interest and degrade accuracy. This can also be seen in Fig. 9(d), where some background points are recognized as part of a vehicle since they project to the same region with the vehicle in 2D [55].

To filter out these tainted points, we design an algorithm to “purify” each object’s point cluster for better 3D bounding box estimation. The details are summarized in Algorithm 1. Chiefly, for each point cluster, it first calculates the depth from all points to the origin of LiDAR coordinate (line 4). Next, it searches for the nearest point to the origin, which most likely represents the boundary of this object and is thus called the critical boundary point (line 5). Then it calculates the distance from all points to the critical boundary point (line 7). Those points close to the critical boundary point are considered to belong to the object itself (line 8). If two few

**Algorithm 1:** Point Filtration

---

**Input :**

- $PC_{old}$ : LiDAR points of all potential objects after point projection.
- $F_T$ : The filtering threshold of Euclidean distance range.
- $M_T$ : The threshold of minimum points in a potential object.
- $S_T$ : The threshold of step size.

**Output:**

- $PC_{new}$ : Filtered LiDAR points.

---

```

1 Function point_filtration( $PC_{old}, F_T, M_T, S_T$ ):
2   for  $PC_i$  in  $PC_{old}$  do
3      $PC_{new}, idx, iter \leftarrow \{\}, [], 0$ ;
4      $depth\_list \leftarrow$  calculate the depth from all points to the origin of LiDAR coordinate;
5      $n_j \leftarrow$  get the nearest point to the origin according to  $depth\_list$ ;
6     while  $sum(idx) < M_T$  do
7        $dist\_list \leftarrow$  calculate the Euclidean distance from all points to  $n_j$ ;
8        $idx = dist\_list < F_T$ ;
9        $n_j \leftarrow$  get the point whose distance to origin is at least  $S_T$  further away;
10       $iter + +$ ;
11      if  $iter == 3$  then break ;
12       $PC'_i = PC_i[idx]$ ;
13       $PC_{new} \leftarrow PC_{new} \cup PC'_i$ ;
14   return  $PC_{new}$ ;

```

---

points are filtered this way, it suggests that the critical boundary point may not be the actual boundary of this object, which can happen when for instance vehicles are close to each other. We then add a small step size  $S_T$  and use the nearest point whose distance to the origin is at least  $S_T$  further away as the new critical point (line 9). We repeat the process until it finds a cluster that has enough points or the number of iteration exceeds three (lines 6 and 11). Fig. 10 depicts an example of the effect of point filtration. The rationale of the algorithm is based on our observation that the points of potential objects are commonly much nearer to the origin than background points. As we measured quantitatively, our point filtration algorithm removed 98% of tainted points. After point filtration, the point cluster of each potential object is clean enough for the following 3D bounding box regression.

**3D Bounding Box Estimation** Moby now strives to estimate each object’s 3D bounding box based on its point cluster. A 3D bounding box is represented by a seven-tuple  $(x, y, z, l, w, h, \theta)$ , including the object’s center  $(x, y, z)$ , size  $(l, w, h)$ , and heading angle  $\theta$  relative to the  $x$  axis on the  $x - y$  plane of LiDAR coordinates. It is challenging to estimate all parameters solely based on the values of points, especially the heading and center, for two main reasons: 1) The point cloud is sparse and irregular; 2) Only part of the object has a point cloud because of the self-occlusion problem [55].

We design a new method to efficiently estimate 3D bounding boxes with high accuracy. For each point cluster that has been associated with an object from the previous LiDAR frame, Moby first obtains the object’s size directly from the estimation of the previous frame. It then estimates the heading angle, and calculates the object center based on size and heading.

Now the heading angle can be obtained from the normal vector of one of the object’s surfaces, if we know which side this surface is. Fig. 11 shows an example of this intuition with different surfaces of an object. Based on this idea, Moby uses the well-known RANSAC algorithm [31] to find a surface first. It iteratively selects three

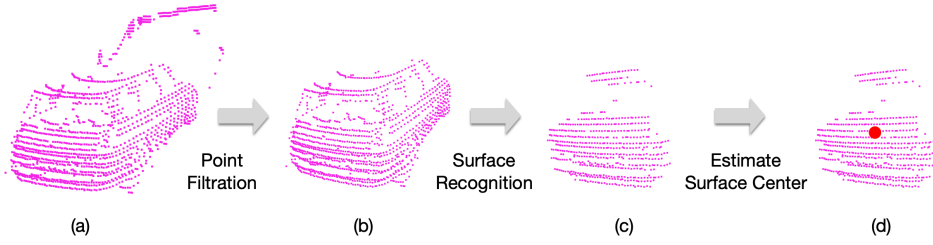


Fig. 10. Key steps of point filtration and 3D bounding box estimation for a point cluster.

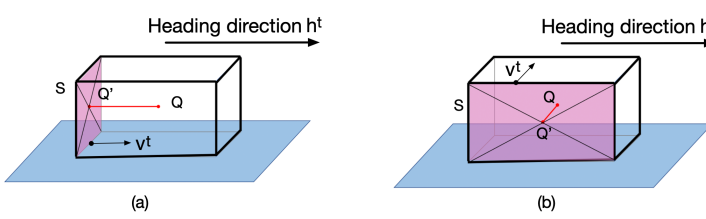


Fig. 11. Two possible situations in bounding box estimation.

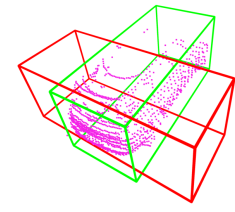


Fig. 12. Compare the number of points inside both situations to determine the correct box.

random points to form a plane until a best-fitting plane is found with the most inliers in it, with its normal vector  $v_t$ . Fig. 10(c) shows the plane it finds on the point filtration output. This plane can be either the front or rear surface as in Fig. 11(a), or the side surface as in Fig. 11(b).<sup>2</sup> To determine the correct heading, Moby calculates the angle between the normal vector  $v^t$  of the surface and the heading direction  $h^{t-1}$  of this object's associated bounding box in the previous LiDAR frame. If the angle is less than a threshold  $\xi$  or greater than  $\pi - \xi$ , it means the normal vector  $v^t$  is nearly parallel to  $h^{t-1}$ , and the surface is the rear or front as shown in Fig. 11(a). Further, since the object moves continuously and is physically impossible to change its heading dramatically in one frame (i.e. 0.1s in KITTI), Moby obtains the heading direction  $h^t$  directly from  $v^t$ :

$$h^t = \begin{cases} v^t, & \text{if angle between } h^{t-1} \text{ and } v^t \text{ is less than } \xi, \\ -v^t, & \text{if angle between } h^{t-1} \text{ and } v^t \text{ is greater than } \pi - \xi \text{ (} v^t \text{ in the opposite direction).} \end{cases} \quad (2)$$

In case  $v^t$  is perpendicular to  $h^{t-1}$  as in Fig. 11(b), we can also easily obtain  $h^t$  by rotating  $v^t$  by either 90 or 270 degrees. The heading angle  $\theta$  is then directly calculated from  $h^t$ .

Lastly, in terms of the object center  $Q$ , Moby estimates it based on the surface center  $Q'$ , the heading angle  $\theta$ , and the object size. Note that the surface center  $Q' = [a, b, c]$  is obtained by averaging the corresponding value of all points in the plane, as shown in Fig. 10(d). Then the object center  $Q$  can be directly calculated by

$$Q = \begin{cases} [a, b, c] + [0.5 * l * \cos \theta, 0.5 * l * \sin \theta, 0], & \text{if angle between } h^{t-1} \text{ and } v^t \text{ is less than } \xi \\ & \text{or greater than } \pi - \xi, \\ [a, b, c] + [0.5 * w * \cos \theta, 0.5 * w * \sin \theta, 0], & \text{otherwise.} \end{cases} \quad (3)$$

<sup>2</sup>Theoretically the found plane can also be the top or bottom surface of a vehicle. Yet in the autonomous driving scenario, LiDAR are installed at the top of the vehicle, and the angle of laser beams makes it very unlikely for the top surface to have more points and then be found by RANSAC. Even when this happens, it can be handled by removing points in the top surface and re-run RANSAC.

Finally we need to consider objects that are not associated with anything in the previous frame after tracking-based association. These are highly likely new objects that first appear in the current frame. Since we no longer have the reliable size information, we use the average length, width and height of all objects to estimate the new object's size. This can be updated after Moby schedules another anchor frame to go through the 3D detector. To estimate the heading angle, Moby uses the same procedure as described above to identify a best-fitting surface based on the point clusters from point filtration. As we no longer have prior knowledge of the heading direction (from the previous LiDAR frame), we adopt an alternative method by calculating the bounding boxes for both possibilities by Eq. (3), and the one that fits more points inside is the final output as shown in Fig. 12.

### 3.4 Frame Offloading Scheduler

As discussed in §2.2, running 3D detectors on the edge device is computationally prohibitive. To utilize the powerful computation resources on server, Moby offloads the intensive computation of 3D object detection model to the server for inference. Unlike existing systems [28, 46] that send every frame to the server, we design a frame offloading scheduler that only offloads necessary frames whose results are required by 2D-to-3D transmission to utilize, thus drastically reducing bandwidth consumption. Specifically, Moby sends two types of frames: 1) test frames are periodically sent to retrieve the detection results to monitor on-board performance; 2) if on-board performance degrades over a threshold, an anchor frame is sent to server for inference while blocking local processing and waiting for the results. Fig. 13 shows the operational flow of frame offloading scheduler. After the workflow is initiated, a test frame is sent after  $N_T$  frames asynchronously, which means Moby still continues on-board processing without waiting the response. When Moby receives the detection results of test frame, an accuracy checker is applied to check the difference between the DNN-based detections and the output of on-board processing. We deem the DNN-based detections as ground truth and calculate the accuracy based on it. If the accuracy is below a threshold  $Q_T$ , it means the performance of 2D-to-3D transformation is degrading and about to fail. Thus, the next frame is assigned as an anchor frame and offloaded to server for accurate 3D object detection, so the subsequent transformations have the most recent 3D information to draw upon. If the accuracy of transformation is still maintained in high quality, Moby will continue on-board processing and re-send a test frame after  $N_T$  frames. The mechanism of test and anchor frames can limit the number of frames offloaded to server, avoiding wasting bandwidth resources while still monitoring the on-board performance.

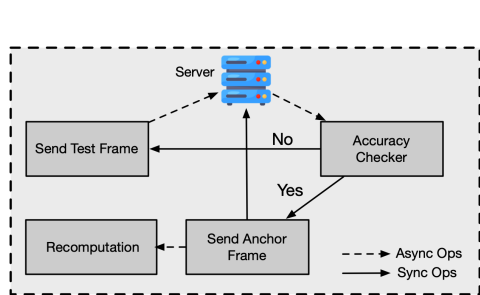


Fig. 13. Overview of frame offloading scheduler.

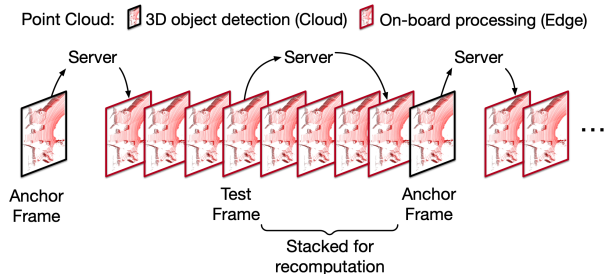


Fig. 14. Illustration of anchor frame, test frame, and re-computation. Note that test frame is asynchronous and does not block on-board processing.

**Recomputation.** Since the process of waiting anchor frame’s result is synchronous, the operational flow of Moby is blocked to wait for the result from server to continue the on-board processing. To make use of the idle computation resources on edge device during the waiting time, we propose a mechanism called recomputation

to recompute the 3D results of past intermediate frames using the results of test frames. As shown in Fig. 14, after sending the test frame, the on-board processing is still ongoing. Some intermediate results such as outputs of instance segmentation model are stacked. When an anchor frame is triggered, the intermediate results and the stale output of test frame are utilized to re-run the 2D-to-3D transformation to recompute 3D bounding boxes. We observe that the recomputation time is much less than the offloading time and is completely hidden without inducing extra latency. This module is optional in real-world deployment, because even though it does not increase overall latency, it will slightly delay the result output of each frame.

#### 4 IMPLEMENTATION

We implement Moby in an edge-server architecture with around ~4K lines of Python code, as shown in Fig. 15. All major components, i.e., tracking-based association, 2D-to-3D transformation and frame offloading scheduler are running on-board, only the 3D object detectors are deployed on server to serve the edge’s inference requests. **Hardware Setup.** We use NVIDIA Jetson TX2 [11] as the edge device, which is a commonly-used commodity mobile module for edge computing (e.g. drone, smart cameras and autonomous delivery vehicles). TX2 is equipped with one 256-core NVIDIA Pascal GPU, one Dual-Core Denver CPU, one Quad-core ARM A57 CPU, and loaded with 8 GB LPDDR4 memory. The server program runs on a desktop with Ubuntu 20.04, which has one NVIDIA GeForce RTX 2080Ti GPU and Intel Core i7-9700K CPU. The edge device and the desktop server are physically connected to a Wi-Fi router and locate in the same local network.

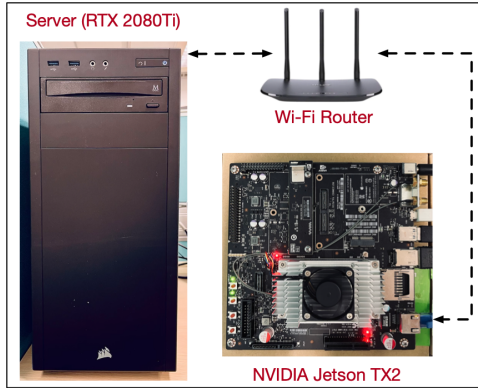


Fig. 15. Our experimental evaluation hardware platform.

**Edge Side.** We implement the edge side of Moby on the Jetson TX2 with installed JetPack SDK 4.6.2. To maximize its performance, we turn on Max-N power mode [12], which fully uses all 6 CPU cores and operates GPU at the highest clock frequency. This mode increases the performance while inevitably sacrificing the power. We also utilize Numba [9], a Just-In-Time (JIT) compiler that translates a subset of Python into fast machine code, to accelerate repeated matrix operation in Moby on the CPU. YOLOv5n [33] is adopted as the default 2D model to execute instance segmentation. Note that the design of Moby is model-agnostic and any 2D object detection model can be used, as we will demonstrate this property in §5.3. The edge device communicates with the server via a TCP connection.

**Server Side.** We deployed OpenPCDet [65] on the desktop server as the inference engine, which is a general PyTorch-based framework for 3D object detection and currently supports a variety of cutting-edge 3D detection techniques. To serve requests, the server also runs a TCP-based socket program to listen to the designated port.

**Parameter Settings.** There are a few parameters in Moby to be determined. We set the association threshold  $I_T$  in tracking-aware association to 0.3. The filtering threshold  $F_T$ , minimum points  $M_T$  and step size  $S_T$  are

empirically set to 4.5, 24 and 12 in point filtration. In the 2D-to-3D transformation, we choose 30 as the default iteration number in the RANSAC algorithm. As for offloading scheduler, the accuracy threshold and the gap of test frame, i.e.  $Q_T$  and  $N_T$ , are set to 0.7 and 4 respectively. We will investigate the sensitivity of key parameters and their impact on the performance in §5.4.

## 5 EVALUATION

We now experimentally evaluate Moby in various aspects by answering the following questions:

- How well does Moby work overall in terms of latency and accuracy?
- How much does each key design choice of Moby contribute to the overall performance gain?
- How sensitive is Moby to the key parameters and 2D instance segmentation models?
- How efficiently does Moby utilize the edge resources in terms of energy and memory consumption?

### 5.1 Experimental Setup

**Evaluation Datasets.** All experiments use the KITTI dataset [32] to evaluate, which is one of the most popular real-world autonomous driving benchmarks. It consists of synced LiDAR scans and front-view camera images with a frequency of 10 FPS. The KITTI dataset provides 3D labels for cars, pedestrians, and cyclists. While currently, we only focus on the most challenging class car in our evaluation as it moves the fastest, and minor design modification is needed for classes like pedestrian and cyclist, which will be discussed in §7.

**Bandwidth Traces.** To evaluate Moby and baseline schemes on realistic network conditions, we use two real-world traces from a broadband dataset provided by FCC [30], and another two 4G/LTE traces collected in Belgium [67]. We deliberately select the four traces that cover different parts of the bandwidth spectrum and are within a normal 4G/LTE performance [1]. They range from 7.76 Mbps to 37.345 Mbps, with an average from 11.89 Mbps to 29.60 Mbps. The statistics of the bandwidth traces are summarized in Table 3. We use Linux TC [7] to control the uploading bandwidth between the edge device and the server by taking the above traces as input.

**Performance Metrics.** We adopt the average end-to-end latency and accuracy as the main performance metrics. The end-to-end latency is defined by the time between the input of point cloud and the output of 3D detection results. As for accuracy, since KITTI provides the human-annotated labels of point cloud, we use them as ground truth to calculate the actual performance of Moby. We consider the object to be successfully detected if the 3D IoU between detection and ground truth  $> 40\%$  (i.e., accurately located). And the accuracy of 3D object detection is measured by the F1 score, i.e. the harmonic mean of precision and recall, which is widely adopted in recent work [19, 28, 61, 75, 77]. The reason why we do not use AP (Average Precision) is that it requires the confidence score to calculate, which is only available in the output of DNN-based detectors.

**Models.** We adopt YOLOv5n from the YOLOv5 codebase[33], one of the classic 2D detection and segmentation techniques, as Moby’s default instance segmentation model. For 3D models, to fairly compare with baselines, Moby uses the same 3D object detection model as baselines. Note that the design of Moby is model-agnostic, any 3D object detection or instance segmentation model can be used, as we will demonstrate this property in §5.2 and §5.4.

### 5.2 Overall Performance

To comprehensively evaluate Moby, we conduct the overall evaluation from two different perspectives: (1) system architecture perspective evaluates how well Moby performs compared to the two typical scenarios, i.e., completely running on board or offloading; (2) alternative approach perspective compares Moby with other accelerating methods and non point cloud-based methods.

**5.2.1 System Architecture perspective.** First, we look at the overall performance benefits from the system architecture perspective. We compare Moby with the following two baselines:

- **Edge Only (EO):** In this scheme, the 3D object detection models are deployed on the edge device and run the inference tasks. The end-to-end latency only involves the inference latency.
- **Cloud Only (CO):** fully offloads the point cloud to the server over 4G/LTE network and runs 3D object detectors on the server. The end-to-end latency involves both transmission and inference latency.

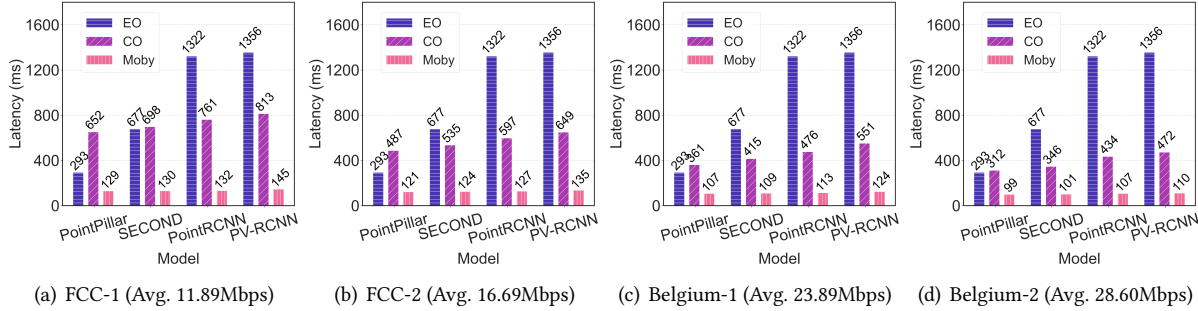


Fig. 16. The end-to-end latency of Moby and compared schemes.

Fig. 16 shows the end-to-end latency comparison between Moby and the baselines using four representative point cloud-based 3D detection models. The details of the four models are described in Table 1. We report the results under the aforementioned four real-world bandwidth traces. We observe that Moby outperforms EO and CO with a large margin of latency reduction ranges from 56.0% to 91.9% for all models. Notably, Moby achieves the lowest latency 99ms with PointPillar in Belgium-2. That matches the frequency of KITTI’s LiDAR that operates at 10 FPS, meaning Moby can run in real time at its best. We also observe the latency gain is much larger for two-stage models, such as PointRCNN and PV-RCNN. That is because their complex architectures pose severe computation burden for the edge device, even for the server with a high-end GPU (over 100ms per frame), which amplify the latency benefits of Moby that is able to perform fast 2D-to-3D transformation on board. Also, we observe that Moby achieves speedup across different bandwidth spectrums. Even for the lowest bandwidth FCC-1, Moby reduces latency by 56.0% compared to running the fastest model PointPillar on board. As the bandwidth increases, the latency improvement reaches 66.2%. We attribute the latency improvement of Moby to three main reasons: (i) Moby replaces the 3D object detector with a much light-weighter 2D model in its pipeline, which dramatically reduces the model inference time; (ii) Moby shifts the burden of 3D object detection to the powerful server, and uses model-free techniques on edge device, such as tracking-based association and 2D-to-3D transformation, to transfer vision semantics to 3D space and generate bounding boxes. (iii) Moby judiciously decides when to offload frames to server that avoids repeated transmission of per frame.

After discussing how Moby can contribute to reducing the end-to-end latency, it is crucial to demonstrate that it has limited impacts upon the accuracy of 3D object detection. Fig. 17 reports the overall accuracy of all schemes. Note that as EO and CO both run 3D object detectors for all frames, they have the same accuracy with the same model. For PointRCNN, we observe that Moby achieves almost the same and a bit higher accuracy: 0.760 vs 0.751. That is because the 2D-to-3D transformation mechanism performs well enough in some cases. While for the other three models, accuracy slightly drops between 0.027 to 0.056. The minor accuracy drop from Moby is because: (i) severe occlusion problem in 2D image hinders the following point projection, which may result in missing objects; (ii) bounding box estimation error, this situation could happen because sometimes point cluster is too sparse to construct an accurate box.

**5.2.2 Alternative Approach Perspective.** Next, we look at the overall performance benefits from the alternative approach perspective. We comprehensively compare Moby with one acceleration method that aims to improve the

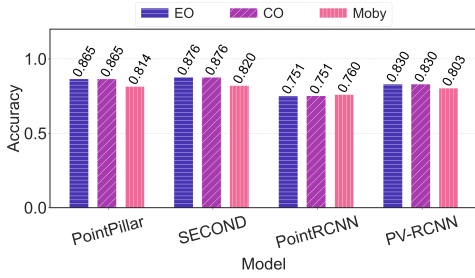


Fig. 17. The 3D detection accuracy of Moby and compared schemes.

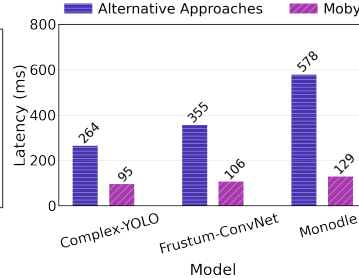


Fig. 18. The end-to-end latency of Moby and alternative approaches.

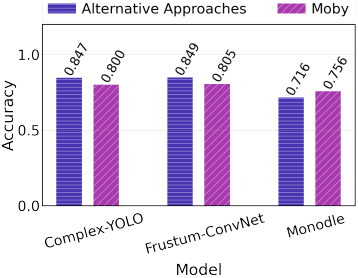


Fig. 19. The 3D detection accuracy of Moby and alternative approaches.

inference efficiency of 3D detection, and another two methods that also leverage image data to insist 3D detection. To fairly compare with these approaches on the edge device, we run Moby fully on board even for anchor frames that need to execute the 3D detection model. Note that the detection model is the same as compared method for fairness. To keep the integrity of Moby’s design, we only offload test frame to server for necessary performance monitoring, and recomputation is disabled.

- **Complex-YOLO** [62]: is a 3D object detection acceleration method. It first converts point cloud to birds-eye-view RGB-map, and uses a light-weight YOLO [57] based architecture to predict 3D boxes with localization and an exact heading of the objects. Complex-YOLO claims it can achieve 50 FPS on an NVIDIA TitanX GPU in its paper [62], which is a powerful desktop-class GPU.
- **Frustum-ConvNet** [71]: is a fusion-based 3D object detector that uses both LiDAR and image. It utilizes 2D region proposals from detection results of images to generate a sequence of frustums on point cloud, thus the 3D detector only needs to run on these frustums that dramatically reduce the search space.
- **Monodle** [48]: Monodle is one of the state-of-the-art image-based 3D detection approaches that only use monocular images. The model is implemented as a multibranch network based on an image feature extraction backbone. Each branch regresses a different quantity in 2D or 3D spaces. 3D bounding boxes are computed by combining the results of each branch based on geometric relationships.

From Fig. 18, we observe that Moby shows significant latency improvement against those three alternative approaches. Even for Complex-YOLO which is specifically designed for 3D detection acceleration, Moby cuts down the latency by 64.0% with only minor accuracy loss. Moby also shows the same advantages compared to the fusion-based approach, Frustum-ConvNet. Notably, compared with the image-based approach Monodle, Moby reduces the latency by 77.6% while improving accuracy by 5.5% at the same time. It’s worth mentioning that here Moby’s accuracy is hindered by Monodle’s low performance compared to other approaches, as the inaccurate output from the detection model directly affects the transformation of Moby. The relatively low accuracy of Monodle is attributed to its inability to detect locations of distant objects effectively, and the problem still haunts existing image-based solutions for 3D object detection [55, 74]. Besides Monodle, we also compare Moby with another two image-based methods, Deep3DBox [50] and Pseudo-LiDAR++ [74]. However, they take 2834ms and 5889ms respectively to run on TX2, which are too slow to execute on the edge device.

### 5.3 Components Analysis

**Contribution of Each Component.** We first break down the system and evaluate the contribution of each key design component in Moby. Here we start from Moby-Local (ML), which runs only on edge device and uses 2D-to-3D transformation (2DT) to generate 3D results without offloading frames to the server. We incrementally

add each component to ML, namely Frame Offloading Scheduler (FOS), Tracking-based Association (TBA), Recomputation (RC). The results are shown in Table 20.

We observe that ML has already achieved decent accuracy without any other techniques, which proves the effectiveness of 2DT. After adding FOS, the accuracy is improved as some frames are sent to server to run 3D object detectors. The offloading latency increases the end-to-end latency while on-board latency remains unchanged. TBA further brings accuracy gain as it helps 2DT to estimate bounding boxes more accurately by using previous detection results. We notice that the end-to-end and on-board latency both drop slightly, which is because TBA reduces the computation overhead of 2DT if boxes are successfully associated. Finally, when RC is added, the accuracy also improves without introducing extra latency, as its time is hidden within the anchor frame as described in §3.4.

**Overheads.** Further, we measure the execution time of key components in Moby that runs on the edge device, including instance segmentation, TBA, FOS, and breakdown of 2DT. We repeat the runs for 300 times and report the average in Fig. 21. It is expected that the inference of instance segmentation takes the longest, accounting for 43.9% of the on-board latency. Then follows the 3D bounding box estimation and point projection with 30.1% and 16.6%, respectively. They are also within expectation because the two steps involve multiple matrix multiplications. For TBA and FOS, they only take 5.14ms and 0.60ms, which are negligible compared to the total latency. Notably, point filtration has only 2.01ms latency, which proves the efficiency of our Algorithm 1.

Components	Accuracy	Latency (ms)	On-board Latency (ms)
ML	0.762	88.44	88.44
ML +FOS	0.787	112.06	89.45
ML +FOS +TBA	0.809	101.50	76.22
ML +FOS +TBA +RC	0.814	99.23	76.29

Fig. 20. The incrementally impact of each component.

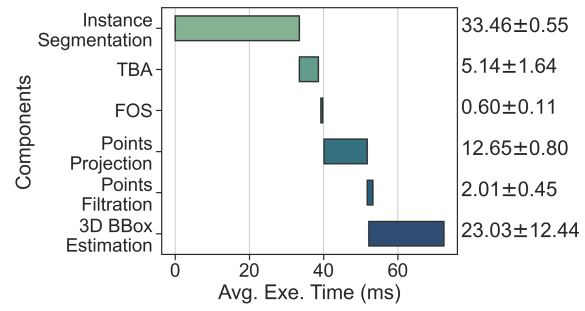


Fig. 21. The avg. execution time of Moby’s main components. Note that here we only report the latency of components that run on the edge device and ignore the offloading latency.

#### 5.4 Microbenchmarks

We now microbenchmark Moby’s performance if we change its key parameters, and also microbenchmark its robustness to 2D models.

**Choosing Iteration Number in RANSAC.** In the 2D-to-3D transformation, the iteration number in RANSAC is a key parameter to perform plane fitting to recognize a surface from the point cluster. Fig. 22(a) and Fig. 22(d) show the accuracy and on-board latency of Moby if we vary the number of iteration number. As we can see, a small number induces less latency but might result in premature or inaccurate surface recognition that misleads the estimation of heading angle and object center. While a larger iteration number makes the plane fitting more robust and meanwhile induce more computation overhead. We experimentally find that 30 is an appropriate iteration number to balance the accuracy and computation cost.

**Sensitivity to Association Criterion.** Fig. 22(b) and Fig. 22(e) test the impact of association criterion, i.e., the IoU threshold that is used to associate two bounding boxes in 2D space as described in §3.2. A larger criterion

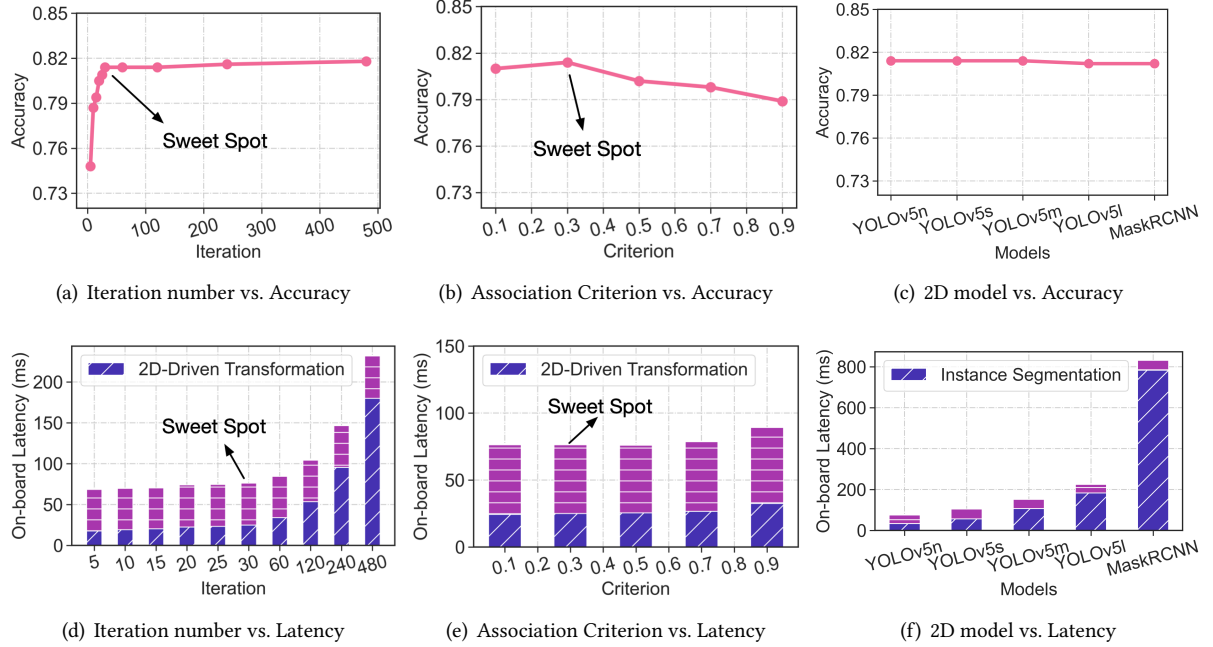


Fig. 22. The impact of key parameters and instance segmentation model on the performance of Moby. Note that here we only consider the on-board latency for clearer comparison.

makes it stricter to connect two bounding boxes, and thus cannot effectively utilize previous 3D results for estimation. We empirically choose 0.3 as the association criterion, as the accuracy gains diminish after it is greater than 0.3. Interestingly, the on-board latency reaches the highest when the criterion is 0.9, because the bounding box estimation is more complex if it is not successfully associated as described in line §14.

**Robustness to 2D Models.** To verify Moby’s robustness to 2D models, we test Moby with other instance segmentation models from YOLOv5 [33] codebase, including YOLOv5s, YOLOv5m, and YOLOv5l. We also test Moby with MaskRCNN [35], one of the classic instance segmentation models and has different feature extractor and network architecture compared to YOLOv5. The results are shown in Fig. 22(c) and Fig. 22(f). We observe that: (i) Moby’s accuracy gains are consistent when using various instance segmentation models; (ii) the on-board latency grows substantially with the increase of model size, while the accuracy almost remains unchanged. The results indicate that a small instance segmentation model is good enough for achieving a decent performance, or in other words, the performance of Moby is not bottlenecked by 2D models. We will further discuss the potential for improvement of Moby in §7.

## 5.5 System Efficiency

Finally, as utilizing resources efficiently is crucial to the applications run on the constrained edge devices [60], we evaluate the system efficiency of Moby.

**Energy Consumption.** We use the built-in Tegrastats Utility [13] of Jetson TX2 to monitor the instant energy consumption for 2 minutes. The sampling rate is 10Hz and we report the average consumption in Fig. 23. Moby achieves the lowest energy consumption and outperforms the baselines significantly. For example, Moby’s power

consumption is only 24.2% of PointPillar. Moby reduces the GPU power and CPU power by 74.3% and 77.3%, respectively. Overall, Moby saves 73% power on average against the four 3D object detection models.

**Memory Footprint.** We also measure the memory footprint of Moby using Tegrastats [13], and the results are shown in Fig. 24. Moby’s overall memory reduction ranges from 17.3% to 48.1% compared to other methods. This is expected because Moby only needs to load a 2D model into the memory that is much smaller than 3D object detection models. Moby shows its competitive advantages in cutting memory footprint, which is even more critical for some entry-level edge devices, such as Jetson Nano [10] that only has 4GB memory shared by both CPU and GPU.

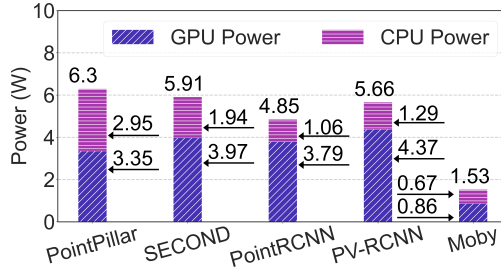


Fig. 23. Energy consumption.

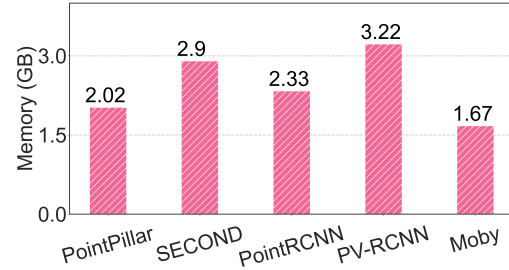


Fig. 24. Memory footprint.

## 6 RELATED WORK

**3D Object Detection.** 3D detectors can be divided into three categories based on input modality. The first and the most common type of 3D detection models use point cloud as input. The key challenge for these models is how to extract features from the sparse point cloud. Voxel-based methods like SECOND [72] first group points into voxels and extract features on voxel level. On the other hand, PointRCNN [59] directly takes the raw point cloud as input and computes a pointwise feature vector. Due to the high cost of LiDAR sensor, a second type of models have been proposed that use only RGB images as input. To compensate for the lack of depth information, Pseudo-Lidar[74] synthesizes LiDAR data based on the image before feeding it to a point cloud model. CaDNN [56] leverages a categorical depth distribution to aid 3d detection. Apart from these two types of models, the third category uses both point cloud and image as input to exploit information in both modalities. CLOCs[53] combines the bounding boxes of a 2D and a 3D detector to refine the results. PointPaining[68] enriches LiDAR data by augmenting each point with 2D image segmentation class score. These models are often heavy as they require two backbones to extract information from both inputs. However, it has been observed that multimodel approaches often only offer marginal performance gain [15, 53, 68]. Currently, point cloud-based methods still dominate 3D detection.

**On-device Inference Acceleration.** Deep learning models are too computationally intensive to deploy on edge devices with limited hardware resources. Lots of efforts have been devoted to accelerating the inference of DNNs on these edge devices, including model compression methods, hardware-based methods and software-based methods. Model compression method utilizes techniques such as network pruning [34, 36, 47], quantization [16, 24], low-rank factorization [26, 63] and knowledge distillation [37, 51] to reduce the model size and perform acceleration. Besides model compression, various work has explored hardware-based methods that design specialized accelerators for hardware, such as FPGA [66, 76] or ASIC [23, 69]. The last line of work is software-based methods. For example, TorchSparse proposes a grouping algorithm to smartly batch the computation workload to reduce irregular computation for sparse point cloud, thus achieving inference speedup [64]; and

many other efforts exploit task-specific optimization [19, 29, 39, 44, 49, 73]. Moby belongs to the last category and is orthogonal to the above work.

**Edge-Cloud Collaboration.** Besides on-device inference, the emergence of edge devices has also sparked much system research in the field of edge-cloud collaboration. Filter-based methods [25, 45, 79] investigate how to leverage edge’s limited computation power to pre-analyze video frames and prune the large data volume before transmission. For example, Elf [79] designs a region proposal prediction algorithm to partition frame into small slices and only offloads partial inference tasks to multiple servers for parallel processing. Reducto [45] uses an on-camera filtering technique to filter out frames that do not contain relevant information for the query. Partition-based methods [38, 40, 78] explore partitioning the DNNs over the edge and cloud to fully utilize the computation resources on both sides. They automatically divide a DNN model into two partitions and deploy the few initial layers to improve inference efficiency. SPINN [43] further incorporates early-exit into DNN partitioning to allow the inference to exit early based on the input complexity. Feedback-based methods [19, 28, 52] rely on the feedback or result from server to assist the local processing. Glimpse [19] periodically sends trigger frames to the server to obtain the object recognition hints to assist local tracking. DDS [28] sends the low-quality video at first and determines where to re-send with high quality driven by the server-side DNN feedback. Unlike the existing work that all targets 2D domain scenarios, our work explores edge-cloud collaboration for more compute-intensive 3D object detection task, which poses server pressure on both edge and server.

## 7 DISCUSSION AND LIMITATIONS

**Occlusion in Images.** Although Moby brings significant latency gain to running 3D object detection models, we notice that the accuracy performance of Moby still has room to improve. One problem that haunts existing image-based 3D object detection and also Moby is the occlusion in 2D images [15, 55]. As we know, an important characteristic of driving environment is occlusion or truncation present in crowded scenes where vehicles can block the view of other agents and themselves [15]. Since 2D-to-3D transformation in Moby is based on the visual perception of images, its accuracy is likely to be affected by the occlusion effect. A possible solution is to integrate an occlusion reasoning module into Moby to handle object missing. While our system can dramatically reduce latency with minor accuracy loss, we have not investigated how much occlusion affects our system’s performance, which is a promising direction for Moby to advance its performance in the future.

**Generalization to Other Classes.** While Moby is mainly evaluated on the 3D detection task of cars, it can be generalized to other 3D detection tasks, such as pedestrians and cyclists. For these tasks, minor design modification is needed in the 2D-to-3D transformation module to estimate the bounding box accurately. For example, because pedestrians and cyclists are smaller than cars, their object centers can be simply calculated by averaging the value of all points in the point cluster. Other task-specific design for the pipeline is also needed to maximize its benefit. We expect Moby achieves similar performance gains in these scenarios, as it can be applied similarly to leverage 2D models for 3D object detection to accelerate inference. We leave this part as future work.

## 8 CONCLUSION

We have presented Moby, a novel framework for accelerating 3D object detection on edge devices. Moby creatively proposes the 2D-to-3D transformation that is capable of transferring vision semantics to 3D space and referring to previous detection results to construct 3D bounding boxes swiftly and accurately. Furthermore, an offloading scheduler is designed to judiciously decide when to offload frame to server for inference, orchestrating the computation resource of edge and cloud jointly. Our evaluation with the real-world autonomous driving dataset KITTI and a full-fledged implementation running on NVIDIA Jetson TX2 shows that, Moby achieves the end-to-end latency reduction by up to 91.9% with only modest accuracy drop. The latency superiority of Moby is consistent across a wide range of state-of-the-art 3D detection models. It supports running at 10 FPS on TX2 that

matches the scanning frequency of LiDAR in KITTI. Noticeably, Moby is also energy-efficient by cutting down power consumption and memory usage by 72.8% and 34.1% on average.

## REFERENCES

- [1] 2020. Average 4G Speed: How Fast Is 4G LTE Compared To 4G+?. <https://commsbrief.com/average-4g-speed-how-fast-is-4g-lte-compared-to-4g/>.
- [2] 2023. 3D Object Detection on KITTI Cars Moderate. <https://paperswithcode.com/sota/3d-object-detection-on-kitti-cars-moderate>.
- [3] 2023. bz2 – Support for bzip2 compression. <https://docs.python.org/3/library/bz2.html>.
- [4] 2023. gzip – Support for gzip files. <https://docs.python.org/3/library/gzip.html>.
- [5] 2023. Jetson TX2 GPU vs GeForce RTX 2080 Ti. <https://technical.city/en/video/GeForce-RTX-2080-Ti-vs-Jetson-TX2-GPU>.
- [6] 2023. Jetson TX2 GPU vs Tesla A100. <https://technical.city/en/video/Tesla-A100-vs-Jetson-TX2-GPU>.
- [7] 2023. Linux Traffic Control (TC). <https://linux.die.net/man/8/tc>.
- [8] 2023. lzma – Compression using the LZMA algorithm. <https://docs.python.org/3/library/lzma.html>.
- [9] 2023. Numba. <https://numba.pydata.org/>.
- [10] 2023. NVIDIA Jetson Nano Developer Kit. <https://developer.nvidia.com/embedded/jetson-nano>.
- [11] 2023. NVIDIA Jetson TX2 Developer Kit. <https://developer.nvidia.com/embedded/jetson-tx2>.
- [12] 2023. NVIDIA Jetson TX2 NVP model. [https://developer.ridgerun.com/wiki/index.php/NVIDIA\\_Jetson\\_TX2\\_NVP\\_model](https://developer.ridgerun.com/wiki/index.php/NVIDIA_Jetson_TX2_NVP_model).
- [13] 2023. Tegrastats Utility. [https://docs.nvidia.com/drive/drive\\_os\\_5.1.6.1L/nvvib\\_docs/DRIVE\\_OS\\_Linux\\_SDK\\_Development\\_Guide/Utilities/util\\_tegrastats.html](https://docs.nvidia.com/drive/drive_os_5.1.6.1L/nvvib_docs/DRIVE_OS_Linux_SDK_Development_Guide/Utilities/util_tegrastats.html).
- [14] 2023. zlib – Compression compatible with gzip. <https://docs.python.org/3/library/zlib.html>.
- [15] Eduardo Arnold, Omar Y Al-Jarrah, Mehrdad Dianati, Saber Fallah, David Oxtoby, and Alex Mouzakitis. 2019. A Survey on 3D Object Detection Methods for Autonomous Driving Applications. *IEEE Transactions on Intelligent Transportation Systems* 20, 10 (2019), 3782–3795.
- [16] Benoit Jacob, et al. 2018. Quantization and Training of Neural Networks for Efficient Integer-arithmetic-only Inference. In *Proc. IEEE CVPR*.
- [17] Alex Bewley, Zongyuan Ge, Lionel Ott, Fabio Ramos, and Ben Upcroft. 2016. Simple online and realtime tracking. In *Proc. IEEE ICIP*. 3464–3468. <https://doi.org/10.1109/ICIP.2016.7533003>
- [18] Romil Bhardwaj, Zhengxu Xia, Ganesh Ananthanarayanan, Junchen Jiang, Nikolaos Karianakis, Yuanchao Shu, Kevin Hsieh, Victor Bahl, and Ion Stoica. 2022. Ekyia: Continuous Learning of Video Analytics Models on Edge Compute Servers. In *Proc. USENIX NSDI*.
- [19] Tiffany Yu-Han Chen, Lenin Ravindranath, Shuo Deng, Paramvir Bahl, and Hari Balakrishnan. 2015. Glimpse: Continuous, Real-Time Object Recognition on Mobile Devices. In *Proc. ACM SenSys*.
- [20] Xiaozhi Chen, Kaustav Kundu, Ziyu Zhang, Huimin Ma, Sanja Fidler, and Raquel Urtasun. 2016. Monocular 3D Object Detection for Autonomous Driving. In *Proc. IEEE/CVF CVPR*.
- [21] Xiaozhi Chen, Huimin Ma, Ji Wan, Bo Li, and Tian Xia. 2017. Multi-view 3D Object Detection Network for Autonomous Driving. In *Proc. IEEE/CVF CVPR*.
- [22] Yukang Chen, Yanwei Li, Xiangyu Zhang, Jian Sun, and Jiaya Jia. 2022. Focal Sparse Convolutional Networks for 3D Object Detection. In *Proc. IEEE/CVF CVPR*.
- [23] Yunji Chen, Tao Luo, Shaoli Liu, Shijin Zhang, Liqiang He, Jia Wang, Ling Li, Tianshi Chen, Zhiwei Xu, Ninghui Sun, et al. 2014. Dadiannao: A Machine-Learning Supercomputer. In *2014 47th Annual IEEE/ACM International Symposium on Microarchitecture*. IEEE, 609–622.
- [24] Matthieu Courbariaux, Itay Hubara, Daniel Soudry, Ran El-Yaniv, and Yoshua Bengio. 2016. Binarized Neural Networks: Training Deep Neural Networks with Weights and Activations Constrained to +1 or -1. *arXiv preprint arXiv:1602.02830* (2016).
- [25] Kaikai Deng, Dong Zhao, Qiaoyue Han, Shuyue Wang, Zihan Zhang, Anfu Zhou, and Huadong Ma. 2022. Geryon: Edge Assisted Real-time and Robust Object Detection on Drones via mmWave Radar and Camera Fusion. *Proc. ACM IMWUT* 6, 3 (2022), 1–27.
- [26] Misha Denil, Babak Shakibi, Laurent Dinh, Marc'Aurelio Ranzato, and Nando De Freitas. 2013. Predicting Parameters in Deep Learning. *Advances in neural information processing systems* 26 (2013).
- [27] Chao Dong, Chen Change Loy, Kaiming He, and Xiaoou Tang. 2015. Image Super-Resolution Using Deep Convolutional Networks. *Proc. IEEE TPAMI* 38, 2 (2015), 295–307.
- [28] Kuntai Du, Ahsan Pervaiz, Xin Yuan, Aakanksha Chowdhery, Qizheng Zhang, Henry Hoffmann, and Junchen Jiang. 2020. Server-driven Video Streaming for Deep Learning Inference. In *Proc. ACM SIGCOMM*.
- [29] Biyi Fang, Xiao Zeng, and Mi Zhang. 2018. NestDNN: Resource-aware Multi-tenant On-device Deep Learning for Continuous Mobile Vision. In *Proc. ACM MobiCom*.
- [30] Federal Communications Commission. 2022. Measuring Broadband America. <https://www.fcc.gov/general/measuring-broadband-america>.

- [31] Martin A Fischler and Robert C Bolles. 1981. Random Sample Consensus: A Paradigm for Model Fitting with Applications to Image Analysis and Automated Cartography. *Communications of the ACM* 24, 6 (1981), 381–395.
- [32] Andreas Geiger, Philip Lenz, and Raquel Urtasun. 2012. Are We Ready for Autonomous Driving? The KITTI Vision Benchmark Suite. In *Proc. IEEE/CVF CVPR*.
- [33] Glenn Jocher, et al. 2022. ultralytics/yolov5: v7.0 - YOLOv5 SOTA Realtime Instance Segmentation. <https://doi.org/10.5281/zenodo.7347926>
- [34] Song Han, Huizi Mao, and William J Dally. 2015. Deep Compression: Compressing Deep Neural Networks with Pruning, Trained Quantization and Huffman Coding. *arXiv preprint arXiv:1510.00149* (2015).
- [35] Kaiming He, Georgia Gkioxari, Piotr Dollár, and Ross Girshick. 2017. Mask R-CNN. In *Proc. IEEE ICCV*.
- [36] Yihui He, Xiangyu Zhang, and Jian Sun. 2017. Channel Pruning for Accelerating Very Deep Neural Networks. In *Proc. IEEE/CVF ICCV*.
- [37] Geoffrey Hinton, Oriol Vinyals, Jeff Dean, et al. 2015. Distilling the Knowledge in a Neural Network. *arXiv preprint arXiv:1503.02531* (2015).
- [38] Hyuk-Jin Jeong, Hyeon-Jae Lee, Chang Hyun Shin, and Soo-Mook Moon. 2018. IONN: Incremental Offloading of Neural Network Computations from Mobile Devices to Edge Servers. In *Proc. ACM SoCC*. 401–411.
- [39] Shiqi Jiang, Zhiqi Lin, Yuanchun Li, Yuanchao Shu, and Yunxin Liu. 2021. Flexible High-resolution Object Detection on Edge Devices with Tunable Latency. In *Proceedings of the 27th Annual International Conference on Mobile Computing and Networking*. 559–572.
- [40] Yiping Kang, Johann Hauswald, Cao Gao, Austin Rovinski, Trevor Mudge, Jason Mars, and Lingjia Tang. 2017. Neurosurgeon: Collaborative Intelligence Between the Cloud and Mobile Edge. *ACM SIGARCH Computer Architecture News* 45, 1 (2017), 615–629.
- [41] Harold W Kuhn. 1955. The Hungarian method for the assignment problem. *Naval research logistics quarterly* 2, 1-2 (1955), 83–97.
- [42] Alex H Lang, Sourabh Vora, Holger Caesar, Lubing Zhou, Jiong Yang, and Oscar Beijbom. 2019. Pointpillars: Fast Encoders for Object Detection from Point Clouds. In *Proc. IEEE/CVF CVPR*.
- [43] Stefanos Laskaridis, Stylianos I Venieris, Mario Almeida, Ilias Leontiadis, and Nicholas D Lane. 2020. SPINN: synergistic progressive inference of neural networks over device and cloud. In *Proc. ACM MobiCom*.
- [44] Jingzong Li, Libin Liu, Hong Xu, Shudeng Wu, and Chun Jason Xue. 2023. Cross-Camera Inference on the Constrained Edge. In *Proc. IEEE INFOCOM*.
- [45] Yuanqi Li, Arthi Padmanabhan, Pengzhan Zhao, Yufei Wang, Guoqing Harry Xu, and Ravi Netravali. 2020. Reducto: On-Camera Filtering for Resource-Efficient Real-Time Video Analytics. In *Proc. ACM SIGCOMM*.
- [46] Luyang Liu, Hongyu Li, and Marco Gruteser. 2019. Edge Assisted Real-time Object Detection for Mobile Augmented Reality. In *Proc. ACM MobiCom*.
- [47] Zhuang Liu, Mingjie Sun, Tinghui Zhou, Gao Huang, and Trevor Darrell. 2018. Rethinking the Value of Network Pruning. *arXiv preprint arXiv:1810.05270* (2018).
- [48] Xinzhu Ma, Yinmin Zhang, Dan Xu, Dongzhan Zhou, Shuai Yi, Haojie Li, and Wanli Ouyang. 2021. Delving Into Localization Errors for Monocular 3D Object Detection. In *Proc. IEEE/CVF CVPR*.
- [49] Akhil Mathur, Nicholas D Lane, Sourav Bhattacharya, Aidan Boran, Claudio Forlivesi, and Fahim Kawsar. 2017. DeepEye: Resource Efficient Local Execution of Multiple Deep Vision Models using Wearable Commodity Hardware. In *Proceedings of the 15th Annual International Conference on Mobile Systems, Applications, and Services*. 68–81.
- [50] Arsalan Mousavian, Dragomir Anguelov, John Flynn, and Jana Kosecka. 2017. 3D Bounding Box Estimation Using Deep Learning and Geometry. In *Proc. IEEE/CVF CVPR*.
- [51] Ravi Teja Mullapudi, Steven Chen, Keyi Zhang, Deva Ramanan, and Kayvon Fatahalian. 2019. Online Model Distillation for Efficient Video Inference. In *Proc. IEEE/CVF ICCV*.
- [52] Vinod Nigade, Ramon Winder, Henri Bal, and Lin Wang. 2021. Better never than late: Timely edge video analytics over the air. In *Proc. ACM SenSys*.
- [53] Su Pang, Daniel Morris, and Hayder Radha. 2020. CLOCs: Camera-LiDAR object candidates fusion for 3D object detection. In *Proc. IEEE/RSJ IROS*.
- [54] Charles R Qi, Wei Liu, Chenxia Wu, Hao Su, and Leonidas J Guibas. 2018. Frustum Pointnets for 3D Object Detection from RGB-D Data. In *Proc. IEEE/CVF CVPR*.
- [55] Rui Qian, Xin Lai, and Xirong Li. 2022. 3D Object Detection for Autonomous Driving: A Survey. *Pattern Recognition* (2022).
- [56] Cody Reading, Ali Harakeh, Julia Chae, and Steven L Waslander. 2021. Categorical depth distribution network for monocular 3d object detection. In *Proc. IEEE/CVF CVPR*.
- [57] Joseph Redmon and Ali Farhadi. 2017. YOLO9000: Better, Faster, Stronger. In *Proc. IEEE/CVF CVPR*.
- [58] Shaoshuai Shi, Chaoxu Guo, Li Jiang, Zhe Wang, Jianping Shi, Xiaogang Wang, and Hongsheng Li. 2020. Pv-rcnn: Point-Voxel Feature Set Abstraction for 3d Object Detection. In *Proc. IEEE/CVF CVPR*.
- [59] Shaoshuai Shi, Xiaogang Wang, and Hongsheng Li. 2019. Pointrcnn: 3d Object Proposal Generation and Detection from Point Cloud. In *Proc. IEEE/CVF CVPR*.

- [60] Weisong Shi, Jie Cao, Quan Zhang, Youhuizi Li, and Lanyu Xu. 2016. Edge Computing: Vision and Challenges. *IEEE internet of things journal* 3, 5 (2016), 637–646.
- [61] Xian Shuai, Yulin Shen, Yi Tang, Shuyao Shi, Luping Ji, and Guoliang Xing. 2021. milliEye: A Lightweight mmWave Radar and Camera Fusion System for Robust Object Detection. In *Proc. ACM IoTDI*.
- [62] Martin Simony, Stefan Milzy, Karl Amendey, and Horst-Michael Gross. 2018. Complex-yolo: An Euler-Region-Proposal for Real-Time 3D Object Detection on Point Clouds. In *Proceedings of the European Conference on Computer Vision (ECCV) Workshops*.
- [63] Cheng Tai, Tong Xiao, Yi Zhang, Xiaogang Wang, et al. 2015. Convolutional Neural Networks with Low-rank Regularization. *arXiv preprint arXiv:1511.06067* (2015).
- [64] Haotian Tang, Zhijian Liu, Xiuyu Li, Yujun Lin, and Song Han. 2022. TorchSparse: Efficient Point Cloud Inference Engine. *Proc. of MLSys* (2022).
- [65] OpenPCDet Development Team. 2020. OpenPCDet: An Open-source Toolbox for 3D Object Detection from Point Clouds. <https://github.com/open-mmlab/OpenPCDet>.
- [66] Yaman Umuoglu, Nicholas J Fraser, Giulio Gambardella, Michaela Blott, Philip Leong, Magnus Jahre, and Kees Vissers. 2017. Finn: A Framework for Fast, Scalable Binarized Neural Network Inference. In *Proceedings of the 2017 ACM/SIGDA international symposium on field-programmable gate arrays*. 65–74.
- [67] J. van der Hooft, S. Petrangeli, T. Wauters, R. Huysegems, P. R. Alface, T. Bostoen, and F. De Turck. 2016. HTTP/2-Based Adaptive Streaming of HEVC Video Over 4G/LTE Networks. *IEEE Communications Letters* 20, 11 (2016), 2177–2180.
- [68] Sourabh Vora, Alex H Lang, Bassam Helou, and Oscar Beijbom. 2020. Pointpainting: Sequential Fusion for 3D Object Detection. In *Proc. IEEE/CVF CVPR*.
- [69] Hanrui Wang, Zhekai Zhang, and Song Han. 2021. SpAtten: Efficient Sparse Attention Architecture with Cascade Token and Head Pruning. In *Proc. IEEE HPCA*.
- [70] Yan Wang, Wei-Lun Chao, Divyansh Garg, Bharath Hariharan, Mark Campbell, and Kilian Q Weinberger. 2019. Pseudo-lidar From Visual Depth Estimation: Bridging the Gap in 3D Object Detection for Autonomous Driving. In *Proceedings of the IEEE/CVF Conference on Computer Vision and Pattern Recognition*.
- [71] Zhixin Wang and Kui Jia. 2019. Frustum Convnet: Sliding Frustums to Aggregate Local Point-Wise Features for Amodal 3D Object Detection. In *Proc. IEEE/RSJ IROS*.
- [72] Yan Yan, Yuxing Mao, and Bo Li. 2018. Second: Sparsely Embedded Convolutional Detection. *Sensors* 18, 10 (2018), 3337.
- [73] Juheon Yi, Sunghyun Choi, and Youngki Lee. 2020. EagleEye: Wearable Camera-based Person Identification in Crowded Urban Spaces. In *Proc. ACM MobiCom*.
- [74] Yurong You, Yan Wang, Wei-Lun Chao, Divyansh Garg, Geoff Pleiss, Bharath Hariharan, Mark Campbell, and Kilian Q Weinberger. 2019. Pseudo-lidar++: Accurate Depth for 3D Object Detection in Autonomous Driving. *arXiv preprint arXiv:1906.06310* (2019).
- [75] Ben Zhang, Xin Jin, Sylvia Ratnasamy, John Wawrzynek, and Edward A Lee. 2018. Awstream: Adaptive Wide-area Streaming Analytics. In *Proc. ACM SIGCOMM*.
- [76] Chen Zhang, Peng Li, Guangyu Sun, Yijin Guan, Bingjun Xiao, and Jason Cong. 2015. Optimizing FPGA-based Accelerator Design for Deep Convolutional Neural Networks. In *Proceedings of the 2015 ACM/SIGDA international symposium on field-programmable gate arrays*. 161–170.
- [77] Haoyu Zhang, Ganesh Ananthanarayanan, Peter Bodik, Matthai Philipose, Paramvir Bahl, and Michael J Freedman. 2017. Live Video Analytics at Scale with Approximation and Delay-Tolerance. In *Proc. USENIX NSDI*.
- [78] Shigeng Zhang, Yinggang Li, Xuan Liu, Song Guo, Weiping Wang, Jianxin Wang, Bo Ding, and Di Wu. 2020. Towards Real-time Cooperative Deep Inference over the Cloud and Edge End Devices. *Proc. ACM IMWUT* 4, 2 (2020), 1–24.
- [79] Wuyang Zhang, Zhezhi He, Luyang Liu, Zhenhua Jia, Yunxin Liu, Marco Gruteser, Dipankar Raychaudhuri, and Yanyong Zhang. 2021. Elf: Accelerate High-resolution Mobile Deep Vision with Content-aware Parallel Offloading. In *Proc. ACM MobiCom*.
- [80] Yin Zhou and Oncel Tuzel. 2018. Voxelnet: End-to-end Learning for Point Cloud Based 3D Object Detection. In *Proc. IEEE/CVF CVPR*.